Structure investigation of the (100) surface of the orthorhombic Al13Co4 crystal

Rafik Addou, Emilie Gaudry, Thomas Deniozou, Marc Heggen, Michael Feuerbacher, P. Gille, Yuri Grin, Roland Widmer, Oliver Gröning, Vincent Fournée, et al.

Structure investigation of the (100) surface of the orthorhombic $Al_{13}Co_4$ crystal

R. Addou, E. Gaudry, and Th. Deniozou*
Department CP2S, Institut Jean Lamour (UMR7198 CNRS-Nancy-Université-UPV-Metz), Ecole des Mines, Parc de Saurupt, 54042 Nancy Cedex, France

M. Heggen and M. Feuerbacher
Institut für Festkörperforschung, Forschungszentrum Jülich, 52425 Jülich, Germany

P. Gille
Department of Earth and Environmental Sciences, Crystallography Section, LMU, Theresienstr. 41, D-80333 München, Germany

Yu. Grin
Max-Planck-Institut für Chemische Physik fester Stoffe, Nöthnitzer Str. 40, 01187 Dresden, Germany

R. Widmer and O. Gröning
EMPA, Nanotech @ Surfaces, Feuerwerkerstraße 39, CH-3602 Thun, Switzerland

V. Fournée, J.-M. Dubois, and J. Ledieu†
Department CP2S, Institut Jean Lamour (UMR7198 CNRS-Nancy-Université-UPV-Metz), Ecole des Mines, Parc de Saurupt, 54042 Nancy Cedex, France

(Received 9 March 2009; published 23 July 2009)

We present a detailed study of the (100) surface of the orthorhombic $Al_{13}Co_4$ crystal using both experimental and *ab initio* computational methods. This complex metallic alloy is an approximant of the decagonal Al-Ni-Co quasicrystalline phase. After sputter-annealing preparation of the surface at 1073 K, the low-energy electron diffraction pattern recorded exhibits a pseudotenfold symmetry with lattice parameters consistent with those of the bulk model. At this stage, scanning tunneling microscopy (STM) measurements reveal two different types of surface terminations. A comparison between these two surface structures and the bulk planes indicate that the terminations correspond either to an incomplete puckered layer (P) or to an incomplete flat layer (F). At 1173 K, the majority of the surface consists of P layer terminations. STM images calculated from our proposed surface model are in good agreement with experimental images. X-ray photoelectron diffraction patterns and single scattering cluster calculations further confirm that the local atomic arrangements present in the bulk model are preserved within the near-surface region.

DOI: 10.1103/PhysRevB.80.014203 PACS number(s): 61.44.Br, 68.35.bd, 68.37.Ef

I. INTRODUCTION

Quasicrystals[1] and approximants belong to the class of intermetallic compounds known as complex metallic alloys (CMAs).[2] The complex crystallographic structure of CMA is based on highly symmetric clusters (elementary building blocks) that decorate large unit cells. The latter may contain up to some thousands of atoms.[3] Quasicrystal samples represent the ultimate case where the size of the unit cell can be considered as infinite.

Over the last fifteen years, the surface structures of icosahedral and decagonal quasicrystals have been intensively studied both from an experimental and a theoretical viewpoint.[4] One major task has been to understand the interplay that exists between their fascinating crystallographic structure and the unusual physical properties measured for surfaces of Al-based CMAs (high hardness, low coefficient of friction, etc.).[5] With the growth of single element quasiperiodic monolayers on quasicrystalline templates, it has been recently possible to show how the electronic structure of a thin film was influenced by its aperiodic structure.[6] Due to the structural complexity inherent to the aperiodic order, approximant phases have often been introduced to model their parent quasicrystal and to perform calculations requiring periodic boundary conditions, and therefore a finite unit cell. For instance, approximant structures have been employed successfully to understand the electronic charge-density distribution at the surface of the icosahedral Al-Pd-Mn quasicrystal.[7] From *ab initio* calculations, simulated scanning tunneling microscopy (STM) images have been generated and they nicely reproduce the local motifs observed on the experimental STM images recorded on quasicrystalline surfaces.[8] This agreement validates further the use of such periodic crystals to model aperiodic structures.

Up to now, the surface study of only one approximant crystal has been reported using STM and low-energy electron diffraction (LEED).[9,10] The analysis carried out on the ξ'-Al-Pd-Mn surface revealed that large flat terraces are separated by a minimal step height that corresponds to half the period along the pseudotenfold (p-10f) axis. This indicates preferential surface termination at specific atomic layers, which are related by a mirror plane. The incomplete topmost surface layers and the atomic fine structures imaged by STM can be interpreted using planes perpendicular to the p-10f axis of the bulk structure model. The fine structure imaged by STM on a single terrace can be interpreted using

the bulk structure model and reveals the existence of an incomplete top layer that consists of decagonal rings of atoms decorating the orthorhombic unit cell. These decagonal rings of atoms are part of the three-dimensional (3D) cluster units used to describe the ξ' phase.[9]

Recent achievements in the growth of centimeter-sized single crystals[11] have allowed the investigation of other CMA surfaces. Here we report the study of the (100) surface of the orthorhombic $Al_{13}Co_4$ approximant STM, LEED, ultraviolet (UPS) and x-ray photoelectron spectroscopy (XPS), x-ray photoelectron diffraction (XPD), and *ab initio* density-functional calculations. The model of the bulk structure has been proposed by Grin *et al.*[12] and is presented in Sec. II. Following the description of the experimental details in Sec. III, the surface preparation along with the identification of the different surface terminations will be explained in Sec. IV. The calculated electronic density of states (DOS) at the Fermi level and the measured valence band will be compared in Sec. V. From *ab initio* calculations, simulated STM images will allow us to interpret our STM measurements. We demonstrate that the most preferred surface termination is related to an incomplete puckered layer of the bulk structure in the topmost surface plane.

II. MODEL OF THE BULK STRUCTURE

The $Al_{13}Co_4$ sample is an approximant of the decagonal Al-Ni-Co quasicrystal,[13–15] whereas the ξ'-Al-Pd-Mn sample has a structure related to the icosahedral Al-Pd-Mn quasicrystals.[16,17] This orthorhombic crystal belongs to the space-group $Pmn2_1$ and has a unit cell containing 102 atoms (78 Al and 24 Co atoms) with the following lattice parameters (Pearson's symbol *o*P102): $a=8.158$ Å, $b=12.342$ Å, and $c=14.452$ Å.[12,18–20] Its bulk structure has been investigated using x-ray single-crystal and powder-diffraction techniques.[12] The $Al_{13}Co_4$ structure is related to several other complex metallic alloys such as the monoclinic $Al_{13}Fe_4$ (Refs. 21 and 22) and other $Al_{13}Co_4$ (Ref. 23) phases, and the $Al_{13}(Pd,Fe)_4$ (Ref. 24) and the ϵ-Al_3Co (Ref. 13) phases. The bulk structure of this approximant is described by the stacking along the [100] direction of two types of layers, a flat (F) and a puckered (P) plane, separated by a mean distance of 2.0 Å. These layers have a p-10f symmetry and appear in the following sequence: $F_{0.0}P_{0.25}F_{0.5}P_{0.75}$, where $P_{0.75}$ and $P_{0.25}$ are mirrored against $F_{0.5}$. The F layer contains 17 Al and 8 Co atoms. The P layer contains 22 Al and 4 Co atoms, and it is therefore slightly Al rich compared to the F layer and denser by one atom. All atomic sites are fully occupied in this model.

The structure of a single F layer can be described by a tiling composed of pentagons and rhombi obtained by connecting Co atoms in the plane. The pentagonal tiles are decorated in two different manners: either by five Al atoms forming a highly distorted pentagon or by an Al-centered pentagon forming a decagonal ring with the Co pentagon [Fig. 1(a)]. The connection between the Co pentagons is completed by one type of rhombus decorated by atoms belonging to both pentagonal tiles. As proposed by Henley,[25] the structure along the [100] direction of the $Al_{13}Co_4$ crystal

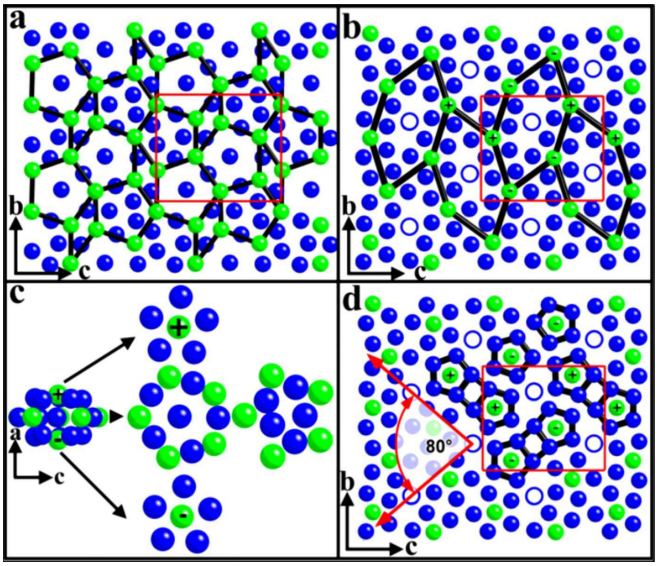

FIG. 1. (Color online) The structure of the orthorhombic $Al_{13}Co_4$ crystal (Ref. 12) is presented along the [100] direction. Solid black (blue) spheres correspond to Al atoms, open circles to Al atoms referenced as glue atoms, and gray (green) spheres to Co atoms. The orthorhombic unit cell is outlined by a rectangle. By connecting Co atoms, (a) a tiling composed of pentagons and rhombi is drawn on the flat layer and (b) a tiling made of elongated hexagons (edge length around 6.5 Å) is superimposed on the puckered layer. The basic building block of the bulk structure is the so-called pentagonal bipyramid (PB) clusters (Refs. 14, 15, and 25). Stacked along this p-10f axis, the PB clusters form pentagonal channels. (c) Description of the 23 atoms PB cluster: (left) a three-dimensional view of the complete PB cluster. The labels (+) and (–) outlined the Co atoms belonging to the top and bottom caps, (middle) dissected cluster showing the Al-centered flat layer with a top and bottom six-atom cap, and (right) the PB junction layer. (d) Within the puckered layer, each cobalt is surrounded by five Al atoms. Depending on the height of the Co atoms [(+) or (–)] within the puckered planes, two sets of bipentagonal motifs are present. A bipentagonal motif is formed by two adjacent alike caps. The edge lengths of the individual pentagons shown on (d) range from 2.66 to 3.05 Å.

can be described using the so-called "pentagonal bipyramid" (PB) cluster as a basic building block [left of Fig. 1(c)]. The PB is a 23 atom cluster containing 16 Al and 7 Co atoms. This three-dimensional atomic arrangement can be dissected into three layers [center of Fig. 1(c)]; an Al-centered equatorial layer consisting of a decagonal ring of alternating Al and Co atoms is capped (top and bottom) by two six-atom puckered layers consisting of small Al pentagons centered by Co atom.[14] Along the [100] direction, the PB clusters alternate with "junction" layers [right of Fig. 1(c)]. Hence, the two pentagons drawn on Fig. 1(a) correspond either to the equatorial or to the junction layers discussed above.

Regarding the P layer [Fig. 1(b)], the connection of Co atoms leads to a tiling composed of a unique elongated hexagon. The hexagonal tiles pointing in two different directions are rotated from each other by 36°. Each Co atom is surrounded by a pentagon composed of five Al atoms. These small pentagons highlighted in Fig. 1(d) correspond either to

the bottom or top caps of the PB cluster. Hence the Co atoms sit either on top or below (labeled, respectively, "+" and "−") the smallest Al pentagons. Consequently, the structure of the *P* layer can be understood as being composed mainly of bottom and top caps of the PB cluster linked by extra Al atoms labeled "glue" atoms [Fig. 1(d)]. At this stage it is worth mentioning that a bipentagonal motif (for instance made by two bottom caps) would be rotated by 80° from one puckered layer to the next one.

III. EXPERIMENTAL DETAILS

The $Al_{13}Co_4$ samples ($Al_{76.5}Co_{23.5}$ at. %) used in this experiment have been grown by the Jülich and the Munich group using the Czochralski method from Al-rich solutions. Crystal growth was done by pulling along the [100] direction using native seeds.[11] The crystals are oriented using back reflection Laue x-ray diffraction and are cut perpendicular to their [100] direction. The surfaces have been mechanically polished using diamond paste with decreasing grain size down to 1/4 μm and using Syton® for the final polishing cycles. At this stage, the appearance of the samples is mirrorlike. After insertion in ultrahigh vacuum (UHV), the preparation of the samples consists of cycles of Ar^+ sputtering and annealing between 1073 and 1173 K. The Ar ion-beam energy is progressively reduced from 1.5 to 1.0 kV and the sputtering cycle lasts 20 min. The base pressure of the system is 5×10^{-11} mbar. As explained later on (see Sec. IV A), the annealing time is varied between 40 min and 2 h per cycle. The temperature of the sample is monitored using an infrared optical pyrometer with the emissivity set to 0.35. The electronic structure of the sample is investigated using XPS and UPS while the overall surface structure is assessed by low-energy electron diffraction. The sample is considered clean when the XPS spectra show no traces of contaminants. The local atomic arrangement is probed using an Omicron variable-temperature atomic force microscope (AFM)/STM operated in the STM mode at room temperature. In a separate UHV chamber (EMPA Thun), XPD measurements have been carried out using nonmonochromatized Al K_α radiation and a modified Omicron photoelectron spectrometer equipped with an EA 125 HR electron analyzer operated in constant analyzer energy mode. The spectrometer has been calibrated to the Au $4f_{7/2}$ binding energy of 83.8 eV. Prior to XPD measurements, the structural quality of the surface is verified using LEED.

IV. EXPERIMENTAL RESULTS

A. Surface preparation

After annealing the sample to 1103 K for 1 h, the LEED pattern is sharp with a low background [Fig. 2(a)]. The surface structure is orthorhombic with the ratio of the unit-cell dimensions ($\frac{c}{b}=1.186$) similar, within the accuracy of our measurements, to those reported by Grin *et al.*[12] ($\frac{c}{b}=1.171$). Compared to other *p*-10*f* surfaces of approximants,[9,26] the *p*-10*f* symmetry within the LEED patterns recorded is less noticeable. As we will see later on, the *p*-10*f* symmetry is very pronounced in the local structure probed by XPD.

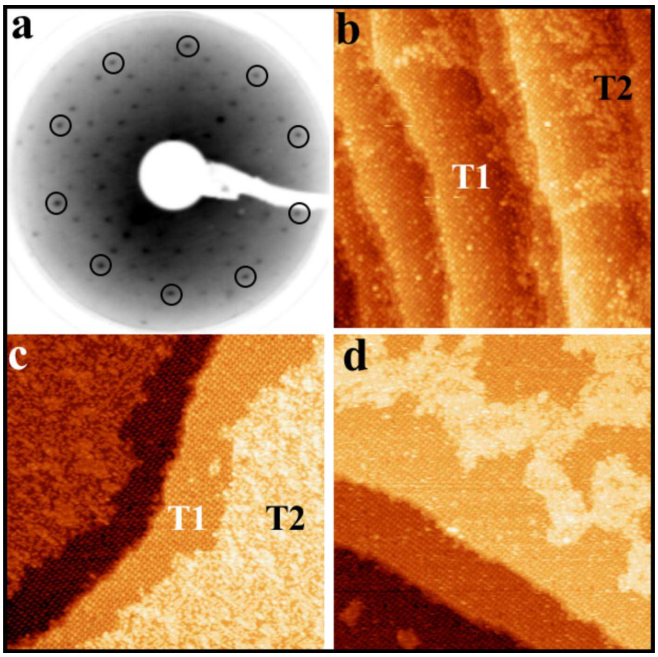

FIG. 2. (Color online) (a) LEED pattern (inverted contrast for clarity) recorded at 80 eV on the surface annealed to 1103 K for 1 h. (b)–(d) 100×100 nm^2 STM images showing the terrace and step morphology for different annealing time and temperatures: (b) $T=1115$ K for $t=1$ h, (c) $T=1115$ K for $t=2$ h, and (d) $T=1165$ K for $t=1$ h. The two types of terminations are labeled T1 and T2 on (b) and (c).

After annealing to 1115 K, STM images [Fig. 2(b)] reveal atomically flat terraces of various widths separated by a single-step height. The latter is equal to 4.2 ± 0.2 Å, which corresponds to half of the lattice parameter ($a/2$) along the [100] direction. High-resolution STM images (not shown here) reveal that the surface structure is similar on all terraces investigated and this termination is labeled T1 on Fig. 2(b). On terraces of width greater than 20 nm, patches of an incomplete surface termination (labeled T2) decorate the upper step edges of the terraces. As shown on Fig. 2(c), increasing the annealing time to 2 h leads to the formation of larger terraces. Now, two distinct terminations are easily distinguishable at the surface. The one closer to the step edge (height=$a/2$) is attributed to T1 and the remaining part of the surface is assigned to T2 [see Fig. 2(c)]. The mean height difference between T1 and T2 is measured at 2.2 ± 0.2 Å, which corresponds to the distance between the flat and the puckered layer in the bulk model. The roughness calculated on both terminations using the root-mean-square height (Z_{rms}) are 0.30 and 0.57 Å for T1 and T2, respectively. Following this surface preparation, the step edges are always T2 deficient. Hence, T1 is only observed on the lower and upper sides of the step edges over a 30-nm-wide region. As shown in Fig. 2(d), a drastic change in the surface morphology is observed when annealing the sample to 1165 K for 1 h. At this temperature, T2 is preferentially desorbed, leaving T1 as the dominant surface plane. The complete evaporation of T2 has been achieved by annealing the $Al_{13}Co_4$ to 1173 K for 2 h. However, this marks the start of the evaporation of T1 as indicated by the presence of depressions across the top most

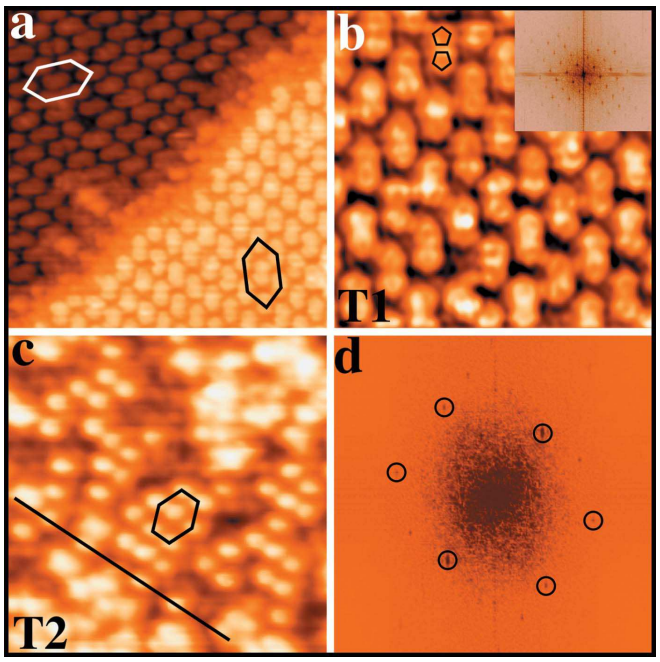

FIG. 3. (Color online) (a) 20×20 nm^2 high-resolution STM image presenting two successive terraces separated by a single-step height equal to $a/2$. The elongated hexagons (longest edge equal to 19 Å) are rotated from one puckered layer to the next one by 80°. (b) Atomically resolved STM image (10×10 nm^2) recorded from T1. Bipentagonal motifs are highlighted on the image [Inset: FFT calculated from T1 termination shown on (b)]. (c) Atomically resolved STM image (10×10 nm^2) measured on T2. The arrangements of bright features are highlighted by an atomic line and a hexagonal motif. (d) Corresponding FFT calculated from a (30×50 nm^2) region of T2. Within the orthorhombic mesh, six intense spots forming an elongated hexagon are circled.

surface layer. The LEED patterns recorded during these different surface preparations are qualitatively identical but drastic changes have been observed within the intensity distribution of the diffraction peaks.

B. Investigation of the surface structure

We now turn into the identification of the atomic structures for both surface terminations using higher magnification STM images. At first [see Fig. 3(a)], the structure observed on T1 can be described using a centered elongated hexagon. The orientation of this hexagon is different on successive terraces and an angle of 80° is measured between the two possible alignments. From atomically resolved STM images, it appears that the center and the vertices of this hexagon are decorated by bipentagonal motifs resembling those presented in Fig. 1(d). The dimensions of individual pentagon and of the unit mesh are consistent with those from the puckered layer (x=0.25 or x=0.75). This is further confirmed by the fast Fourier transform (FFT) [inset of Fig. 3(b)] calculated from the T1 region, which exhibits an orthorhombic structure with the lattice-parameter dimensions ($b=12.6\pm0.3$ Å and $c=14.5\pm0.1$ Å) expected from the bulk structural model.[12] However, only one set of bipentagonal features pointing in one direction within each plane is preserved at the surface. These pentagons correspond either to bottom or top caps of the PB cluster. As it will be demonstrated further using simulated STM images, the presence of both sets of bipentagonal motifs would have led to a full puckered layer with a completely different topography [see Fig. 7(a) for instance]. Consequently, the puckered layer is not as dense as in the bulk model and atomic desorption (both Al and Co atoms) is encountered during the surface preparation. The rising question is which out of the two possible pentagons remain at the surface. Additional analytical tools (for instance *ab initio* calculations) will be required to discriminate between the two possibilities. An atomically resolved STM image from a region of T2 is shown on Fig. 3(c). This termination is not complete as revealed by the presence of several holes and of irregularly decorated unit cells. From the densest area, atomic lines and local hexagonal-like features are readily distinguishable [outlined on Fig. 3(c)]. Although not complete, T2 is well ordered as indicated by the FFT presented in Fig. 3(d). Similarly, the dimensions of the orthorhombic unit cell are comparable to those measured on T1. Within the diffraction spots observed on the FFT pattern, six intense spots are arranged in a hexagonal manner [see Fig. 3(d)]. In the following section, we propose a structural model to explain our STM observations on the T2 termination and the intensity distribution obtained within the FFT.

C. Structural model of both surface terminations

The thorough inspection of several STM images allows us to identify a recurrent atomic arrangement within the T2 region [inset of Fig. 4(a)]. The analysis of denser area observed on T2 is hindered by a limited STM resolution. To understand its orientation and position with respect to the crystal structure, a mesh representing the surface orthorhombic unit cell has been drawn on the T1 region and has been extended over the T2 layer [Fig. 4(a)]. To a first approximation, this motif or superstructure is described as an oblique surface net with four atoms or clusters of atoms at the positions (0,0), $(\frac{1}{2},0)$, $(\frac{1}{4},\frac{1}{2})$, and $(\frac{3}{4},\frac{1}{2})$ with respect to the sample orthorhombic unit cell [inset of Fig. 4(b)]. Squashed hexagons as the one presented on Fig. 3(c) can be generated from this basic unit. The corresponding diffraction pattern of this superstructure has been calculated and is presented in Fig. 4(b). The intensity distribution of the Bragg spots has been simulated and varies according to the following structure factor:

$$S(h,k) = 1 + \exp(i\pi h) + \exp\left[i\left(\frac{\pi}{2}h + \pi k\right)\right] + \exp\left[i\left(\frac{3}{2}\pi h + \pi k\right)\right]. \quad (1)$$

Around the central spot, the next six most intense peaks form a hexagonal motif [Fig. 4(b)]. The overall pattern obtained from our proposed superstructure is in good agreement both qualitatively and quantitatively with the calculated FFT from the T2 region [see Fig. 3(d)].

Using the grid shown in Fig. 4(a) as a reference, it has been possible to superimpose part of the STM image repre-

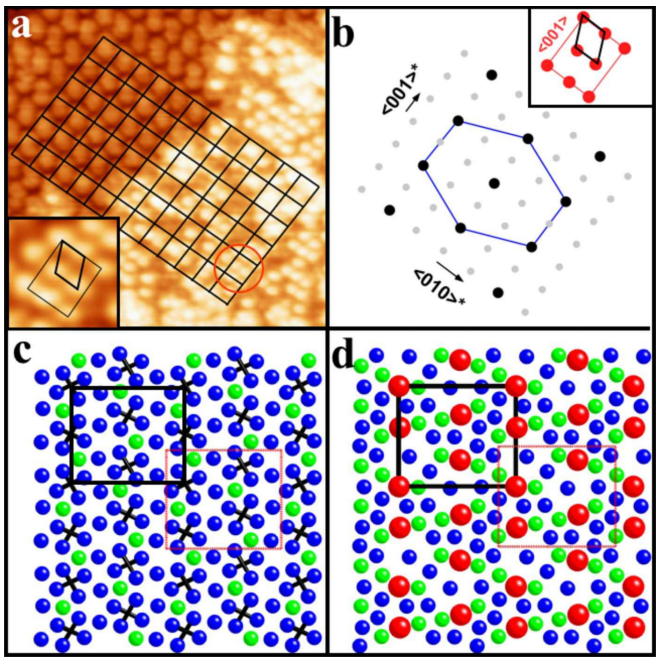

FIG. 4. (Color online) (a) 20×20 nm^2 STM image showing both T1 and T2 terminations. The orthorhombic lattice determined on the T1 region has been extended over the T2 layer. Inset (3×3 nm^2): magnification of the atomic arrangement circled on the STM image. The oblique net is outlined on this motif, which is often observed within the T2 structure. (b) Inset: schematic representation of the correspondence between the oblique net and the orthorhombic unit cell. Calculated diffraction pattern from the superstructure described in the inset. The most (black) and less (gray) intense Fourier spots are indicated in the pattern. (c) Superposition of the oblique net (crosses) and the complete puckered layer [black (blue): Al atoms, gray (green) Co atoms]. (d) Correspondence between the crosses and atomic positions within the flat layer of the bulk model. The largest spheres represent Al5, Al6, Al7, and Al8 in the bulk model (Ref. 12) [atoms labeled as in (c)].

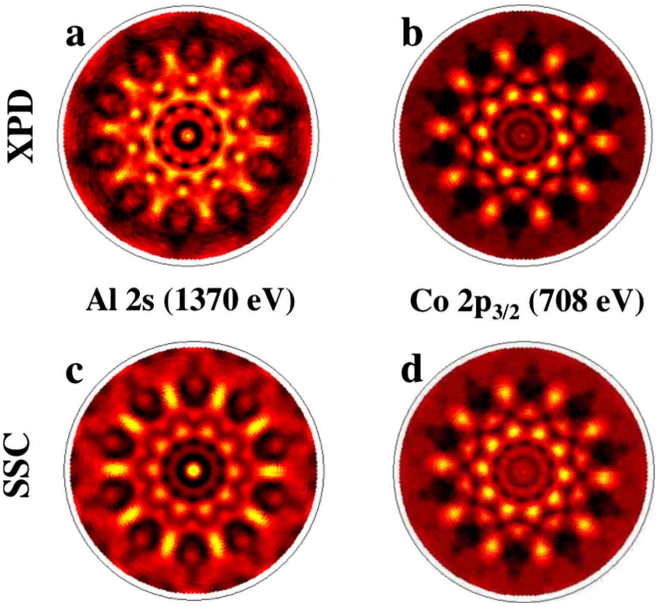

FIG. 5. (Color online) Experimental XPD patterns of (a) Al $2s$ and (b) Co $2p_{3/2}$ core levels measured on the $Al_{13}Co_4$ (100) surface with an Al K_α (1486.7 eV) x-ray source. (c) and (d) Single scattering cluster simulations for Al $2s$ (E_{Kin}=1370 eV) and (d) Co $2p_{3/2}$ (E_{Kin}=708 eV) emission based on a cluster of 3016 atoms derived from the bulk model (Ref. 12) described in Fig. 1.

senting the T2 layer over the T1 region (not shown here). The projection of the two terminations is presented on Fig. 4(c) where crosses indicate the estimated position of the oblique net over a complete puckered layer from the bulk model. The superposition of the two structures shows that the crosses are positioned between Al pentagons defined as the bottom and top caps of the PB cluster [see Figs. 1(c) and 1(d)]. Hence, the crosses are located on top of interstitial sites of the puckered layer. Next, the structure of the flat layer situated above the puckered layer in the bulk model is investigated. In particular, we seek for any correspondence between the oblique cell and atomic positions within the F layer. As shown on Fig. 4(d), a reasonable fit is identified between the position of crosses and several sites decorated by Al atoms. These atoms are labeled Al5, Al6, Al7, and Al8 by Grin *et al.*,[12] and are represented by the largest spheres in Fig. 4(d). The crosses at midedge position along the ⟨010⟩ direction of the orthorhombic unit cell do not coincidence perfectly with the Al atoms marked by arrows. This small shift could be related to a possible surface relaxation, a consequence of the reduced atomic density of the F layer at the surface. Alternatively, an electronic contribution from the atoms beneath the topmost layer could provide a higher local density of states at the midedge position along the ⟨010⟩ direction. Hence we tentatively assign the decoration of the oblique net by Al atoms belonging to the F layer. If we consider the above measurements (step height, calculated FFT, local atomic arrangement), we believe that T2 corresponds to the incomplete F layer in the bulk model, where the density of the flat layer or T2 at the surface depends on the sample preparation.

We now focus on the potential atomic structure of the T1 termination. To this end, our STM measurements suggest that only one type of bipentagonal motifs is preserved with the topmost layer. Investigation of numerous STM images point also to a desorption of glue atoms [see Figs. 1(b) and 1(c)]. In an attempt to test this hypothesis, the surface has been analyzed using X-ray photoelectron diffraction. The measurements have been carried out after annealing the $Al_{13}Co_4$ crystal to 1073 K for 2 h. As explained in Sec. IV A, the majority of the surface consists of relatively narrow terraces with T1 as the topmost termination. Figures 5(a) and 5(b) exhibit the Al $2s$ and Co $2p_{3/2}$ photoemission line intensities for different angular and polar emission angles, represented in stereographic projection. Normal emission corresponds to the center of the XPD pattern while the outer ring represents an emission angle of 85°, i.e., almost parallel to the crystal surface. The bright and dark contrasts on these stereographic projections indicate high and low intensities, respectively. The XPD patterns measured for both selected emitter (Al $2s$ and Co $2p_{3/2}$) reveal typical features of decagonal symmetry elements. Indeed, several rings of ten equivalent intense spots and a central $10f$ symmetry axis dominate both diffractograms. These decagonal patterns re-

semble the XPD images of Al $2s$ and Co $2p_{3/2}$ emission obtained from the *d*-Al-Ni-Co quasicrystal surface.[27] The diffraction images presented in Figs. 5(a) and 5(b) are also similar to those observed on the decagonal quasicrystal overlayer grown on the fivefold surface of the *i*-Al-Pd-Mn sample.[28] As XPD probes the local real-space environment around the selected emitting atoms, these measurements reveal an average short-range decagonal ordering around the Al and Co atoms at the near surface. From the cluster arrangements described in Sec. II, it is not too surprising to observe these patterns along the p-10f axis of the $Al_{13}Co_4$ surface. To interpret the experimental diffractograms, single scattering cluster (SSC) simulations for the Al $2s$ and Co $2p_{3/2}$ emissions have been performed based on the $Al_{13}Co_4$ structural bulk model available.[12] Following the previous analysis, three separate clusters have been generated to encounter for the different atomic configurations observed at the surface. Hence, the surface of the three models is either terminated by a complete F plane, by a complete P plane, or by an incomplete P layer where only bipentagonal motifs have been preserved as suggested by our experimental and simulated STM images. The cluster used to carry out the calculations consists of 3016 atoms with 358 Al and 136 Co as emitters. The photoelectron intensity maps obtained for each emitter appear similar regardless of the models chosen. As shown on Figs. 5(c) and 5(d), the experimental XPD patterns can be nicely reproduced by the SSC simulations. The latter has been obtained for the incomplete P layer. There is a good agreement between the position and the intensity maxima between the XPD and SSC images. In addition, they both display decagonal rings with ten distinct and equivalent spots. Consequently, the similarity between XPD and SSC patterns suggests that the bulk structure is maintained at the near-surface region. However, it is not possible to discriminate between the preferred topmost surface terminations. To gain more insight into the possible surface structures and into the electronic charge-density distribution, the use of *ab initio* electronic structure calculations is introduced in the following section.

V. ELECTRONIC STRUCTURE CALCULATIONS

In this section, we study the electronic structure of the $Al_{13}Co_4$ crystal. We present electronic DOS calculations and simulations of STM images that we have used to interpret experimental results.

A. Computational details

The present calculations have been performed within the density-functional theory framework. Specifically, we have used (i) the Vienna *ab initio* simulation package (VASP) (Refs. 29 and 30) to determine the geometry of the $Al_{13}Co_4$ (100) system, by a conjugate gradient minimization of the forces acting on the atoms, and (ii) the PWSCF code of the QUANTUM ESPRESSO distribution[31] to calculate the density of states and simulate the STM images. Both codes solve the Kohn-Sham equations in a plane-wave basis. Our calculations are made within the Perdew-Burke-Ernzerhof approximation for the exchange-correlation functional.[32] Ultrasoft pseudopotential has been used for cobalt[33] while norm-conserving pseudopotentials have been employed for aluminum.[34] The DOS calculations are carried out at a fixed cutoff energy of 400 eV, and the irreducible Brillouin zone was sampled by $4k$ points.

The density of states of the bulk $Al_{13}Co_4$ alloy is calculated from the relaxed structural model. The starting structure is the experimentally derived model detailed in Ref. 12. The cell geometry, its volume, and the atomic positions were allowed to relax in the process. The resulting structure is still described by an orthorhombic cell built on the [100] (a =8.207 Å), [010] (b=12.403 Å), and [001] (c=14.420 Å) vectors. Using the supercell technique, (100) surfaces of $Al_{13}Co_4$ were simulated by repeated slabs separated by a vacuum region in the z direction. Several surface terminations are considered in this study. The simplest model consists of a bulk truncation along the (100) plane. Two cases are examined: in the F_m model the flat layer is selected as the topmost surface layer while in the P_m model the puckered layer is chosen as the surface termination. In the second structural model (labeled P_m^+ model), the puckered layer is selected as the surface layer and only bipentagonal patterns formed by the top caps are preserved at the surface [Co + atoms in Figs. 1(c) and 1(d)]. For the third structural model (labeled P_m^- model), bipentagonal patterns formed this time by the bottom caps of the PB cluster are maintained at the surface [Co − atoms in Figs. 1(c) and 1(d)]. A complete relaxation of all these systems remains a challenging computational task for at least the following reasons: the slab has to be thick enough so that (i) the model represents a termination of the bulk structure in a realistic way and (ii) the bottom surface has no influence on the studied surface. This demands considering generally at least six atomic planes in the slab, which means 153 atoms if the model is built by a bulk truncation along the (100) plane. We have estimated the surface relaxation only in the case of the P_m^+ and P_m^- models. The STM images calculated from these relaxed surfaces are not drastically different from those simulated from the unrelaxed models.

STM images have been simulated using the Tersoff-Hamann approximation[35] where the tunneling current is derived from the local density of states at the Fermi energy and a pointlike tip is considered. Within this model, the constant current STM images are simulated from electronic structure calculations by considering surfaces of constant local density of states integrated over an energy window from E_F to $E_F + V_{bias}$, where V_{bias} is the voltage applied between the sample and the tip. The bias V_{bias} and the tip-sample distance have been chosen to match the experimental settings (V_{bias} =−1.3 V, I=0.08 nA).

B. Calculated DOS and experimental valence band

Calculated partial and total DOS of bulk $Al_{13}Co_4$ are reported in Fig. 6. The density of states contains a pseudogap lying to the left-hand side of the Fermi energy. Here the Fermi energy is taken as the origin for the binding energies. The total DOS shows an intense feature lying at about 2.0 eV

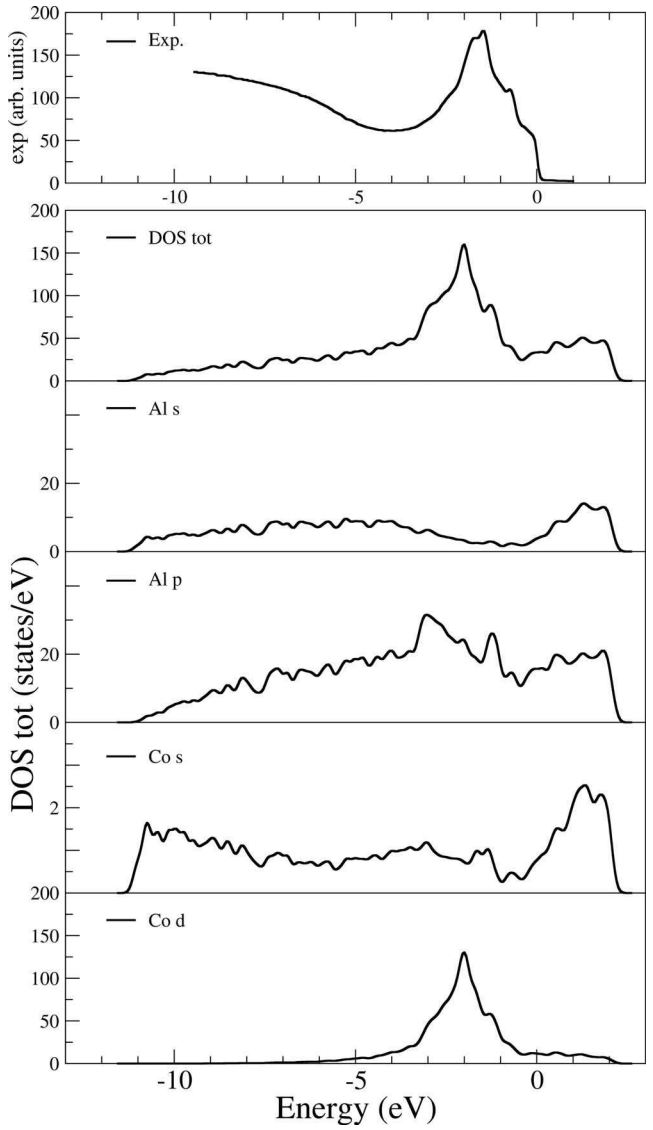

FIG. 6. Calculated partial and local DOS for $Al_{13}Co_4$ crystal. The calculated DOS are compared with the ultraviolet photoelectron spectroscopy measurements (top).

from the Fermi energy. This feature is made mainly from the partial Co *d* states, forming a set of peaks lying between −3.3 and −0.5 eV. The intensity of the Co *s* states is about 85 times lower than the Co *d* states in the occupied region and consequently they do not contribute significantly to the occupied band. Aluminum *s* states are present mainly in the range from −1.0 to −11.2 eV. These later overlap with the Al *p* states leading to a slight *s*-*p* hybridization. At the energy of the intense feature of the partial Co *d* states, a set of peaks is also present in the Al *p* states.

Our results for the DOS are in good agreement with the DOS calculations performed on the *m*-$Al_{13}Co_4$ (Ref. 14) system. Since the orthorhombic *o*P102 and the monoclinic *m*P102 structures of the $Al_{13}Co_4$ crystals share identical local building blocks and differ only in their global arrangement,[14] a similar shape for both DOS was expected.

UPS experiments have been performed to probe the valence band of the $Al_{13}Co_4$ surfaces using He I radiation (21.2 eV). The experimental spectrum is shown in the upper panel of Fig. 6. The spectrum is dominated by the Co *d* levels in the energy range of −0.5−−2.5 eV below the Fermi energy. Some small discrepancies exist between the experimental and the calculated positions of the features. The experimental bands are shifted by about 0.5 eV to lower binding energies compared to the calculated ones. These differences could be due to final-state effects in the photoemission process and/or to a surface effect not taken into account in the calculation of the bulk DOS.

C. Simulated STM images

STM images have been simulated for various structural models of the $Al_{13}Co_4$ (100) surface. These models, which are built using the supercell approach, are made by nonrelaxed slabs composed of four atomic planes and a 9.7-Å-thick vacuum region. We have checked that the same results are obtained with supercells containing six nonrelaxed atomic planes and a 9.4-Å-thick vacuum region. Four structural models have been examined: two models (P_m and F_m) containing 102 atoms and two models (P_m^+ and P_m^-) containing 88 atoms as 14 atoms (2 Co and 12 Al atoms) of the unit cell are removed. Figure 7 [parts (a)–(e)] shows the corresponding STM images calculated from the surface charge-density distribution.

The influence of the surface relaxation on the simulated STM images has been checked only for the P_m^+ and P_m^- models [see Figs. 7(d) and 7(f)]. As the thickness of the slab containing four atomic planes may be too small to support the surface during a relaxation by interatomic forces, a slab containing 139 atoms distributed on six atomic planes ($F_{0.0}P_{0.25}F_{0.5}P_{0.75}F_{1.0}P_{1.25}^{modif}$, where $P_{1.25}^{modif}$ is the incomplete *P* termination) separated by a 9.4-Å-thick vacuum region has been used instead. During the relaxation process, the cell geometry, its volume, and the positions of atoms lying at the first four layers [atoms lying in the surface plane (*S*), in the subsurface (*S*-1), and in planes *S*-2 and *S*-3] were allowed to relax while the positions of atoms lying in the two bottom planes were fixed to model the bulk behavior. The relaxation process was considered to be achieved when the atomic forces for atoms lying in planes *S*, *S*-1, *S*-2, and *S*-3 were less than 0.02 eV/Å. The relaxation did not affect significantly the geometry of the orthorhombic supercell (the norms of the crystal cell vectors are modified by less than 1.7%). The relaxation $\Delta_{ij}^{\%}=\frac{d_{ij}^R-d_{ij}^{NR}}{d_{ij}^{NR}}$, where d_{ij}^R (d_{ij}^{NR}) is the interlayer spacings for the relaxed models (nonrelaxed model) has been evaluated. For the P_m^+ model, the outermost layer spacing is contracted by 9.5% (d_{12}^R=1.72 Å, d_{12}^{NR}=1.90 Å) relative to the bulk interlayer spacing while the spacing of the second and the third planes is expanded by less than 1% (d_{23}^R=2.05 Å, d_{23}^{NR}=2.04 Å). For the P_m^- model, the outermost layer spacing is equal to d_{12}^R=1.88 Å while the spacing of the second and the third planes is d_{23}^R=2.15 Å. The interlayer spacing relaxations calculated here are much larger than those obtained experimentally from LEED analysis[36–39] (0.9–2.2 %) and from generalized gradient approximation calculations[40,41] (1.06–1.35 %) on pure Al(111). However, our results are comparable with the relaxations measured by

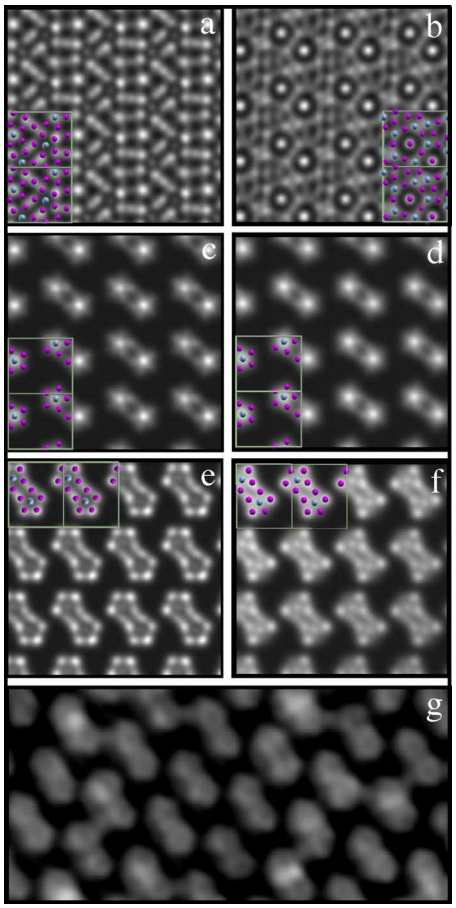

FIG. 7. (Color online) 5×5 nm^2 simulated STM images ($V_{bias}=-1.3$ V) compared to the experimental (5×10 nm^2) STM image recorded with $V_{bias}=-1.3$ V and $I=0.08$ nA (g). The upper simulated images correspond to the (a) puckered and (b) flat planes perpendicular to the [100] direction of the bulk structural model. (c) and (d) show simulated images of the unrelaxed and relaxed P_m^+ (see text) structural models. (e) and (f) Simulated images corresponding to the unrelaxed and relaxed P_m^- structural model, respectively, described in the text.

dynamical LEED analysis (10%) on the tenfold surface of the decagonal Al-Ni-Co quasicrystal.[42] It has to be mentioned that this strong contraction of the uppermost layer does not modify drastically the simulated STM images [see Figs. 7(c) and 7(d)]. In the following, the STM simulations are made with unrelaxed and relaxed structural models.

Figure 7 shows STM images calculated from the surface charge-density distribution obtained for the structural models described in Sec. V A and the experimental STM image recorded with $V_{bias}=-1.3$ V ($I=0.08$ nA). The crystallographic structure of the surface planes is superimposed on the calculated images. Figures 7(a) and 7(b) correspond to two simulated STM images calculated from the complete puckered and flat layers. These terminations have been generated by a cut perpendicular to the [100] direction of the bulk model. The resulting fine details of these simulated images bear no resemblance with the structure of the experimental STM image presented in Fig. 7(g). This drastic difference precludes both complete puckered and flat layers to be surface termination. Figures 7(c)–7(f) have been, respectively, simulated from the structural models containing 88 atoms described in Sec. V A as P_m^+ and P_m^- models. As for the experimental STM image, these simulated images display bipentagonal motifs, all of comparable size and pointing in the same direction. The bright contrasts visible on Figs. 7(c) and 7(d) originate from the position of Co atoms sitting slightly above the Al atoms. Such high intensity in the middle of each pentagonal motif is not observed on Fig. 7(g). However, the best agreement is obtained with Figs. 7(e) and 7(f). For the unrelaxed P_m^- model, the bipentagonal patterns reveal a bright outline and a dark center consistent with our experimental observations. Upon relaxation, the two outermost Al atoms situated at both ends of the pentagonal motifs move slightly inward, hence producing a dimmer contrast. In comparison, the two Co atoms located in the center of the pentagons present a minor outward relaxation. However, they still remain below the mean surface plane and should overall appear as depressions in the bipentagonal motifs. From these observations, we propose that the topmost surface layer consists of bottom caps of the PB cluster [model in Figs. 7(e) and 7(f)] while the top caps are preferentially desorbed upon annealing.

VI. DISCUSSION

At the surface of the $Al_{13}Co_4$ (100) crystal, two different surface terminations have been identified. The area covered by termination T2 depends largely on the surface preparation whereas T1 planes are always present. The complete desorption of the T2 layer can eventually be achieved as explained previously. A strain-related mechanism[43] introduced by surface defects (i.e., step edges) has been observed at the surface of the $Al_{13}Co_4$ crystal. This strain effect is manifested by a systematic depletion of T2 termination ("denuded zone") on the ascending and descending edges of the steps over a relatively wide region. These step edges are similar in shape to those reported on the ξ'-Al-Pd-Mn surface.[9] Hence, the step roughness or diffusivity appears qualitatively lower than on quasicrystal surfaces.[44]

The structural analysis of both surface terminations using LEED, STM, and XPD indicates that there is no evident lateral surface reconstruction. The results obtained using XPS confirm that there is no chemical segregation at the surface of the $Al_{13}Co_4$ crystal. These observations (no segregation) is in favor of a stronger Al-Co interaction strength compared to bonding of similar atoms.[45] Both surface layers can be related to bulk planes although their density is drastically altered (incomplete layers). The surface unit cell of T1 plane is composed of ten Al and two Co atoms compared to 22 Al and 4 Co atoms for a complete puckered layer. It is also frequent to observe an additional Al atom or "glue atom" (i.e., not belonging to the PB cluster) in between bipentagonal motifs. In addition, the atomic decoration of the remaining T2 patches has been attributed to remaining Al atoms from the flat layers. These results reveal that ultimately the Al-richest plane (puckered layer) is favored at the surface. Even after partial desorption, the T1 plane is still largely Al rich. If no reconstruction and no chemical segregation are encountered at the surface, one way to minimize

the surface free energy can be achieved by exposing planes with the lowest surface energy. On all CMA surfaces studied so far, atomic planes have been reported to be laterally bulk terminated. For Al-based CMA, the topmost surface planes always correspond to layers having the highest concentration of Al atoms, i.e., the element possessing the lowest surface energy within the alloy. This selection mechanism of surface plane is also verified for the $Al_{13}Co_4$ crystal.

The $Al_{13}Co_4$ (100) surface presents several similarities with the p-10f surface of the ξ'-Al-Pd-Mn crystal.[9] In both cases, a single-step height equal to half of the lattice parameter along the p-10f axis is measured. The LEED pattern is described as sharp and p-10f symmetric. Each terrace is composed of several atomic terminations. The fine atomic structures observed within terraces are interpreted as originating from incomplete bulk planes. As we know, the atomic structures of both systems are based on elementary atomic clusters as building blocks. Within the incomplete surface layers, part of these clusters is preferentially maintained. Hence, they can be considered as energetically more stable than the surrounding glue atoms. In the case of the $Al_{13}Co_4$ crystal, an additional question arises on why only one type of bipentagonal motif is kept at the surface. Along the p-10f axis, the structure can be visualized as an arrangement of columns of PB clusters. The puckered layer corresponds to a perpendicular cut across these columns. This implies that PB clusters are dissected at different heights and this is manifested by two different bipentagonal patterns within the plane. The selective desorption of one type of bipentagonal feature suggests that PB clusters are relatively independent entities at the surface. Indeed, the shape of the remaining cut clusters is not altered. This apparent stability indicates that the strongest chemical bonds may be localized within the cluster along the columns and not between clusters of separate columns. Although it has been shown that favorable interactions exist between clusters,[46] this difference may be a direct consequence of the reduced symmetry at the surface. Recent studies based on quantum-mechanical calculations[47] supported by nuclear-magnetic-resonance experiments[48] suggest that the Co-Al-Co molecular groups present within the 23 atoms PB cluster should be considered as guests trapped in Al and Co cages of the $Al_{13}Co_4$ complex metallic alloy. The corresponding two Co atoms belonging to such a molecular group are labeled + and − on Fig. 1(c), and the Al atom decorates the center of the flat layer of the PB cluster. Our study suggests that bipentagonal motifs topped with Co + atoms vanish from the topmost surface layer. At the surface, the Co-Al-Co molecular groups are not confined anymore along the [100] direction between cages. It is reasonable to postulate that this break in the symmetry could increase the mobility of the guest within the cage. This could lead to the instability of the bipentagonal motif and explain eventually the observed selective desorption upon annealing of the sample to 1073 K. If the molecular groups or part of it desorb upon annealing, the remaining five Al atoms of the top cap [see Fig. 1(c)] may also evaporate due to a structural instability.

Consequently, the symmetry of the topmost layer is modified due to the reduction in the atomic density. With only one type of bipentagonal motifs preserved, this selection leads eventually to a different intensity distribution within the LEED pattern (reduced p-10f symmetry). However, the local atomic arrangement within the near-surface region exhibits a decagonal symmetry as shown by XPD measurements and SSC calculations.

Finally, the electronic density of states has been calculated for the orthorhombic $Al_{13}Co_4$ crystal. The results are consistent with the DOS calculated for the monoclinic system in previous studies[14] and with the measured valence band. Simulated STM images have been generated and have allowed us to discriminate between different possible surface terminations. The relatively large unit cell and the unusual surface structure reported here should stimulate the use of the $Al_{13}Co_4$ (100) surface in adsorption studies as a highly corrugated potential-energy surface is expected.[49]

VII. CONCLUSIONS

We have investigated the (100) surface of the recently grown orthorhombic $Al_{13}Co_4$ crystal. Atomically flat terraces separated by a step height equal to half of the unit-cell parameter ($a/2$) exhibit two possible surface terminations depending on the annealing time and temperature selected. Both surface layers have been related to incomplete planes present within the bulk structural model. Upon annealing to 1173 K, only one termination that has been attributed to an incomplete puckered layer consisting of 12 atoms per surface unit cell is maintained at the surface. This preferential plane selection leads to a reduced pseudotenfold symmetry of the sharp LEED pattern. Finally, the close match between simulated and calculated STM images validates our proposed surface model.

ACKNOWLEDGMENTS

The European Network of Excellence on "Complex Metallic Alloys," Contract No. NMP3-CT-2005-500145, and the Agence Nationale de la Recherche, Reference No. ANR-08-Blan-0041-01, are acknowledged for their financial support.

*Present address: Fritz- Haber-Institut der Max-Planck-Gesellschaft Abteilung Moleklphysik Faradayweg 4-6, 14195 Berlin, Germany.

†Corresponding author; Ledieu@lsg2m.org

[1] D. Shechtman, I. Blech, D. Gratias, and J. W. Cahn, Phys. Rev. Lett. **53**, 1951 (1984).

[2] *Basics of Thermodynamics and Phase Transitions in Complex Intermetallics*, edited by E. Belin-Ferré (World Scientific, Singapore, 2008).

[3] M. Feuerbacher, C. Thomas, J. P. A. Makongo, S. Hoffmann, W.

Carrillo-Cabrera, R. Cardoso, Y. Grin, G. Kreiner, J.-M. Joubert, T. Schenk, J. Gastaldi, H. Nguyen-Thi, N. Mangelinck-Nöel, B. Billia, P. Donnadieu, A. Czyrska-Filemonowicz, A. Zielinska-Lipiec, B. Dubiel, T. Weber, P. Schaub, G. Krauss, V. Gramlich, J. Christensen, S. Lidin, D. Fredrickson, M. Mihalkovic, W. Sikora, J. Malinowski, S. Brühne, T. Proffen, W. Assmus, M. De Boissieu, F. Bley, J.-L. Chemin, J. Schreuer, and W. Steurer, Z. Kristallogr. **222**, 259 (2007).

[4] H. R. Sharma, M. Shimoda, and A. P. Tsai, Adv. Phys. **56**, 403 (2007).

[5] J. M. Dubois, in *Useful Quasicrystals*, edited by T. K. Wei (World Scientific, Singapore, 2005).

[6] J. Ledieu, L. Leung, L. H. Wearing, R. McGrath, T. A. Lograsso, D. Wu, and V. Fournée, Phys. Rev. B **77**, 073409 (2008).

[7] M. Krajčí and J. Hafner, Phys. Rev. B **71**, 054202 (2005).

[8] M. Krajčí, J. Hafner, J. Ledieu, and R. McGrath, Phys. Rev. B **73**, 024202 (2006).

[9] V. Fournée, A. R. Ross, T. A. Lograsso, J. W. Anderegg, C. Dong, M. Kramer, I. R. Fisher, P. C. Canfield, and P. A. Thiel, Phys. Rev. B **66**, 165423 (2002).

[10] H. R. Sharma, M. Shimoda, V. Fournée, A. R. Ross, T. A. Lograsso, and A. P. Tsai, Phys. Rev. B **71**, 224201 (2005).

[11] P. Gille and B. Bauer, Cryst. Res. Technol. **43**, 1161 (2008).

[12] J. Grin, U. Burkhardt, M. Ellner, and K. Peters, J. Alloys Compd. **206**, 243 (1994).

[13] X. Z. Li and K. Hiraga, J. Alloys Compd. **269**, L13 (1998).

[14] M. Mihalkovič and M. Widom, Phys. Rev. B **75**, 014207 (2007).

[15] E. Cockayne and M. Widom, Philos. Mag. A **77**, 593 (1998).

[16] M. Boudard, H. Klein, M. de Boissieu, M. Audier, and H. Vincent, Philos. Mag. A **74**, 939 (1996).

[17] N. Shramchenko and F. Dénoyer, Eur. Phys. J. B **29**, 51 (2002).

[18] T. Goedecke and M. Ellner, Z. Metallkd. **87**, 854 (1996).

[19] T. Goedecke, Z. Metallkd. **62**, 842 (1971).

[20] B. Grushko and T. Velikanova, CALPHAD: Comput. Coupling Phase Diagrams Thermochem. **31**, 217 (2007).

[21] J. Grin, U. Burkhardt, M. Ellner, and K. Peters, Z. Kristallogr. **209**, 479 (1994).

[22] P. J. Black, Acta Crystallogr. **8**, 43 (1955).

[23] R. C. Hudd and W. H. Taylor, Acta Crystallogr. **15**, 441 (1962).

[24] K. Saito, K. Sugiyama, and K. Hiraga, Mater. Sci. Eng., A **294-296**, 279 (2000).

[25] C. L. Henley, J. Non-Cryst. Solids **153-154**, 172 (1993).

[26] Th. Deniozou, R. Addou, A. Shukla, M. Heggen, M. Feuerbacher, M. Krajčí, J. Hafner, R. Widmer, O. Gröning, V. Fournée, J.-M. Dubois, and J. Ledieu (unpublished).

[27] M. Shimoda, J. Q. Guo, T. J. Sato, and A. P. Tsai, Surf. Sci. **454-456**, 11 (2000).

[28] D. Naumović, P. Aebi, L. Schlapbach, C. Beeli, K. Kunze, T. A. Lograsso, and D. W. Delaney, Phys. Rev. Lett. **87**, 195506 (2001).

[29] G. Kresse and J. Furthmüller, Phys. Rev. B **54**, 11169 (1996).

[30] G. Kresse and J. Furthmüller, Comput. Mater. Sci. **6**, 15 (1996).

[31] S. Baroni, A. Dal Corso, S. de Gironcoli, P. Giannozzi, C. Cavazzoni, G. Ballabio, S. Scandolo, G. Chiaroyyi, P. Focher, A. Pasquarello, K. Laasonen, A. Trave, R. Car, N. Marzari, and A. Kokalj, http://www.pwscf.org

[32] J. P. Perdew, K. Burke, and M. Ernzerhof, Phys. Rev. Lett. **77**, 3865 (1996).

[33] D. Vanderbilt, Phys. Rev. B **41**, 7892 (1990).

[34] N. Troullier and J. L. Martins, Phys. Rev. B **43**, 1993 (1991).

[35] J. Tersoff and D. R. Hamann, Phys. Rev. B **31**, 805 (1985).

[36] H. D. Shih, F. Jona, D. W. Jepsen, and P. M. Marcus, J. Phys. C **9**, 1405 (1976).

[37] H. B. Nielsen and D. L. Adams, J. Phys. C **15**, 615 (1982).

[38] J. R. Noonan and H. L. Davis, J. Vac. Sci. Technol. A **8**, 2671 (1990).

[39] C. Stampfl, M. Scheffler, H. Over, J. Burchhardt, M. Nielsen, D. L. Adams, and W. Moritz, Phys. Rev. B **49**, 4959 (1994).

[40] J. L. F. Da Silva, C. Stampfl, and M. Scheffler, Surf. Sci. **600**, 703 (2006).

[41] A. Kiejna and B. I. Lundqvist, Phys. Rev. B **63**, 085405 (2001).

[42] N. Ferralis, K. Pussi, E. J. Cox, M. Gierer, J. Ledieu, I. R. Fisher, C. J. Jenks, M. Lindroos, R. McGrath, and R. D. Diehl, Phys. Rev. B **69**, 153404 (2004).

[43] J. Stewart, O. Pohland, and J. M. Gibson, Phys. Rev. B **49**, 13848 (1994).

[44] J. Ledieu, E. J. Cox, R. McGrath, N. V. Richardson, Q. Chen, V. Fournée, T. A. Lograsso, A. R. Ross, K. J. Caspersen, B. Unal, J. W. Evans, and P. A. Thiel, Surf. Sci. **583**, 4 (2005).

[45] M. Polak and L. Rubinovich, in *Surface Alloys and Alloy Surfaces*, edited by D. P. Woodruff (Elsevier, Amsterdam, 2002), p. 86.

[46] M. Widom and E. Cockayne, Physica A **232**, 713 (1996).

[47] Yu. Grin, B. Bauer, U. Burkhardt, R. Cardoso-Gil, J. Dolinšek, M. Feuerbacher, P. Gille, F. Haarmann, M. Heggen, P. Jeglič, M. Müller, S. Paschen, W. Schnelle, and S. Vrtnik, EUROMAT 2007: European Congress on Advanced Materials and Processes, Nürnberg, Germany, 2007, Book of abstracts p. 30.

[48] P. Jeglič, M. Heggen, M. Feuerbacher, B. Bauer, P. Gille, and F. Haarmann, J. Alloys Compd. **480**, 141 (2009).

[49] S. Curtarolo, W. Setyawan, N. Ferralis, R. D. Diehl, and M. W. Cole, Phys. Rev. Lett. **95**, 136104 (2005).